Microelectronic Engineering 88 (2011) 2831–2836

Contents lists available at ScienceDirect

Microelectronic Engineering

journal homepage: www.elsevier.com/locate/mee

Accelerated Publication

Local doping of silicon by a point-contact microwave applicator

P. Livshits, V. Dikhtyar, A. Inberg, A. Shahadi, E. Jerby *

Faculty of Engineering, Tel Aviv University, Ramat Aviv 69978, Israel

ARTICLE INFO

Article history:
Received 23 June 2010
Received in revised form 16 March 2011
Accepted 5 April 2011
Available online 22 April 2011

Keywords:
Silicon thermal processing
Thermal-runaway
Silicon doping
pn junctions
Microwaves

ABSTRACT

The feasibility of local doping in silicon by an open-end coaxial applicator with a tip made of the doping material, e.g. aluminum or silver, is studied in this paper. In these experiments, localized microwave power of 100–350 W at 2.45 GHz was applied for ~1 min to obtain doped regions of ~1-mm width and ~0.3-μm depth. Independent measurements of secondary ion mass spectroscopy (SIMS) and junction built-in potential measured by atomic-force microscopy (AFM) were used to estimate the activated doping concentrations in the order of 10^{19} and 10^{22} cm^{-3} for aluminum and silver doping, respectively. Potential barriers (*pn* junctions) of 0.5–0.7 V were measured across the aluminum-doped regions, and *I–V* characteristics were observed. The doping experiments were conducted in air atmosphere, hence oxidation effects were observed as well. The localized-microwave doping concept presented here could be useful in small-scale semiconductor processes, integrated optics, and MEMS applications.

© 2011 Elsevier B.V. All rights reserved.

1. Introduction

Doping processes are essential for the creation of electronic junctions in silicon, and for the manufacturing of semiconductor devices in general [1]. The increasing integration scale and operating speed of electronic devices require shallower junctions with fewer defects and higher surface quality [2]. Hence, they motivate advanced studies of ultra-shallow junction formation by various techniques, such as using ion implantation, flash lamps, plasma discharges, lasers, combination of both plasma and lasers, and chemical vapor deposition [3–11]. Microwaves have been studied for silicon-wafer annealing and doping, and for other related processes including bonding, fast firing, and melting [12–15]. It is noted that besides the major batch manufacturing approach in microelectronics, there is also a need for single wafer or even single device manufacturing techniques [16] which require small-scale processes as presented here.

Considering p-type semiconductors production, aluminum and silver are relatively fast-diffusing acceptors in silicon [17,18]. Their high diffusion coefficients allow manufacturing of semiconductor devices for power applications by rapid thermal processing (RTP) methods [19,20]. The short diffusion time at relatively low temperatures allows the formation of junctions with limited surface damage and lesser contaminants due to the shortened heating time and lower temperatures. Aluminum as a dopant has the ability to getter metallic contaminants and to increase the carrier diffusion length, therefore it has been largely studied for improving the characteristics of solar cells [19]. Nevertheless, the mechanisms of thermal diffusion of aluminum in silicon have not been sufficiently studied. Silver, as another fast-diffusing dopant in silicon, is traditionally used in Schottky metal–semiconductor junctions [21].

Lately, silver doping has been explored for quantum-well formation in silicon [22]. Local doping by tips of scanning tunneling microscope (STM) has been demonstrated recently for patterning highly p-type doped silicon in order to form wires [23] and arrays [24]. The microwave-drill technique [25] enables the localization of microwave energy in a hotspot induced intentionally within the material in a localized thermal-runaway process [26]. In this study, we have modified this microwave RTP technique and employed it to create local doping and oxidation effects in silicon [27]. The next sections introduce the point-contact microwave RTP technique, present experimental results of silicon localized doping and their analysis, and discuss the feasibility of the point-contact microwave technique for local doping in silicon.

2. Experimental setup

In this experiment, the local doping in a silicon matrix is obtained by a point-contact microwave applicator as illustrated in Fig. 1 [28]. The near-field microwaves tend to concentrate in a thermal-runaway process [26,29] underneath the dopant's contact point with the wafer. This effect causes rapid local heating that diffuses the doping material into the silicon within the confined hotspot. The experimental device is illustrated in Fig. 2. The tip made of the doping material is used as the center electrode in contact with the silicon surface. The process is ceased before structural damage or melting occurs at the silicon surface [29], except for

* Corresponding author.
E-mail address: jerby@eng.tau.ac.il (E. Jerby).

0167-9317/$ - see front matter © 2011 Elsevier B.V. All rights reserved.
doi:10.1016/j.mee.2011.04.022

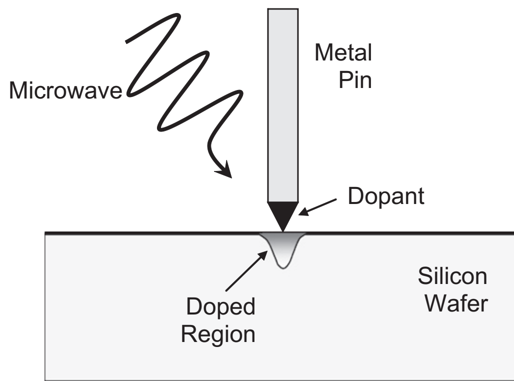

Fig. 1. Local doping in silicon by a point-contact microwave applicator. The microwave energy concentrating underneath the contact point of the dopant with the wafer causes there a rapid thermal-runaway process that diffuses the doping material locally into the silicon.

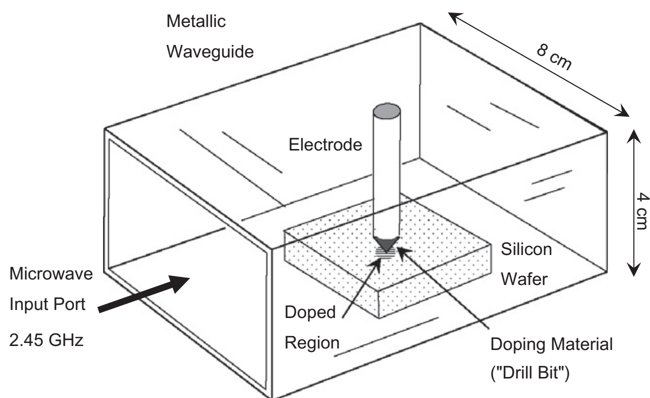

Fig. 2. The experimental setup of the microwave-drill apparatus modified for silicon doping.

the desired local thermal diffusion of the doping material into the silicon in the contact region.

In the experiments presented here, we used tips made of aluminum or silver (99.99% and 99.9998% purity, respectively) in order to diffuse these materials thermally into n-type silicon samples (of 0.37-mm thick, 5-Ωcm resistivity wafers, cut to 20×20 mm^2 area slices). Several experiments were conducted for the sake of comparison with p-type silicon samples (5-Ωcm resistivity, 0.5-mm thickness).

The microwave point-contact applicator shown in Fig. 2 was fed by a 2.45-GHz power-adjustable magnetron source (Alter SM745) in a cascade with an isolator, a directional coupler, and a three-stub impedance-matching tuner. The doping experiments were conducted in various power levels in the range of 100–350 W for a 1-min period each.

The resulting locally doped silicon slices were examined by secondary ion mass spectroscopy (SIMS) and by X-ray photoelectron spectroscopy (XPS) using Physical-Electronics TOF-TRIFT-II and PHI-590, respectively. The electrical characterization across the junction formed in the locally doped silicon was performed with atomic force microscope (AFM, Veeco's Dimension 3100 with a WS×M 4.0 Develop-8 software). Specifically, the latter has been used to measure and image the Contact Potential Difference (CPD), a well common method for potential mapping of Si *pn*-junctions [30,31]. The 4200-SCS Semiconductor Parameter Analyzer of Keithley was employed to measure the *I–V* characteristics. Prior to these tests, the silver doped silicon slices were cleaned by nitric acid in order to remove residues from the silicon surface. The aluminum-doped slices were cleaned by tetra-methyl-ammonium hydroxide.

3. Experimental results

Fig. 3a and b show examples of SIMS profiles for n-type silicon slices locally doped by aluminum (Fig. 3a) and by silver (Fig. 3b) using the point-contact device fed by 350-W microwave power. The penetration profiles shown in these graphs were derived from the SIMS sputtering rate. The silver doping provides a higher concentration than the aluminum doping in these conditions (in accordance with the higher diffusivity of silver into silicon, $\sim 4.10^{-9}$ cm^2/s as compared to $\sim 4.10^{-13}$ cm^2/s for aluminum, both at ~1150 °C [17–19]). Since our experiments were performed in air atmosphere, the localized microwave heating caused also an oxidation of the silicon. The oxide layer is deeper than the doped region in both cases. These results were verified by XPS measurements.

SIMS was used also to examine the effect of the microwave power level on the doping profile in the n-type silicon slices. The results presented in Fig. 4 show that the doped region depth depends almost linearly on the microwave power (the doping depth is defined here as where the SIMS dopant count has reduced to $\sim 10^1$ with no significant noise). At all microwave-power levels, the silver doping was found deeper than the aluminum doping under the same conditions.

The lateral diffusion profile of the silver-doped and aluminum-doped silicon slices were examined by SIMS analyses in various

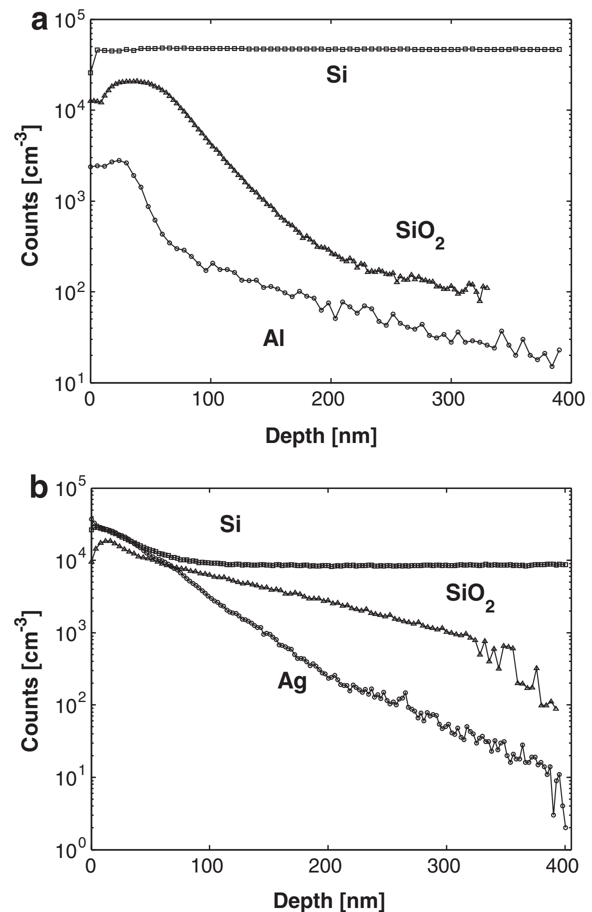

Fig. 3. Secondary ion mass spectroscopy (SIMS) profiles of n-type silicon wafers locally doped by aluminum (a) and silver (b) using a 350-W modified microwave drill.

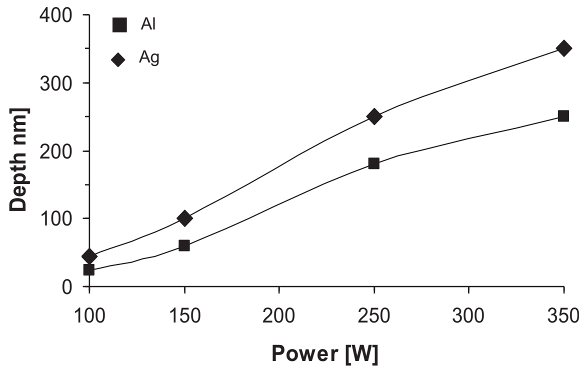

Fig. 4. The penetration depth (counts > 10^1) of silver and aluminum atoms in silicon wafers versus the microwave power applied by the modified microwave drill.

distances from the center of the affected zone. Fig. 5 shows an example for the decrease in the doping depth away from the contact point of the microwave-electrode. A similar reduction in the oxide concentration was observed as well. These results indicate that though a 122-mm wavelength near-field microwave energy has been used, the induced doping effect was localized into a lateral range of <1 mm.

The potential differences were measured in both n-type and p-type silicon slices locally doped by aluminum (both experiments were conducted at the same conditions for the sake of comparison). Fig. 6 shows a measurement of the resulting CPD across the doped regions in the n-type and p-type slices. In the p-type silicon, the resulting potential difference is 0.09 V, whereas in the n-type silicon it exceeds 0.5 V. Fig. 7 shows the potential image of the n-type silicon after the point-contact microwave applicator treatment. The bright area is an aluminum doped region, whereas the dark area is un-doped n-type silicon. The image contrast indicates the potential difference. Maximal voltages of up to 0.7 V have been measured for aluminum doping in an n-type matrix. Since the aluminum dopant acts as an acceptor [18], its p-type doped region forms a larger potential barrier combined with the n-type silicon background. Hence, a *pn*-junction is formed. It should be noted that these results are in a good agreement with those obtained for *pn*-junctions made using ion implantation and thermal diffusion methods [32].

The formation of the *pn*-junction was verified by measuring the *I–V* characteristics of the junction, as presented in Fig. 8. The diode-like behavior is clearly seen in this graph in a comparison to an

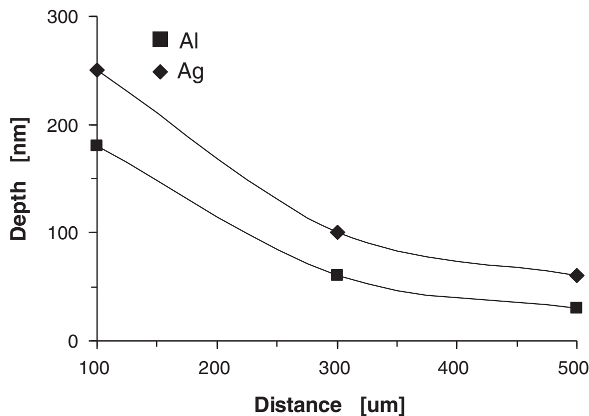

Fig. 5. Lateral diffusion profiles of silver and aluminum in n-type silicon wafer locally doped by the modified microwave drill at a 250 W power level.

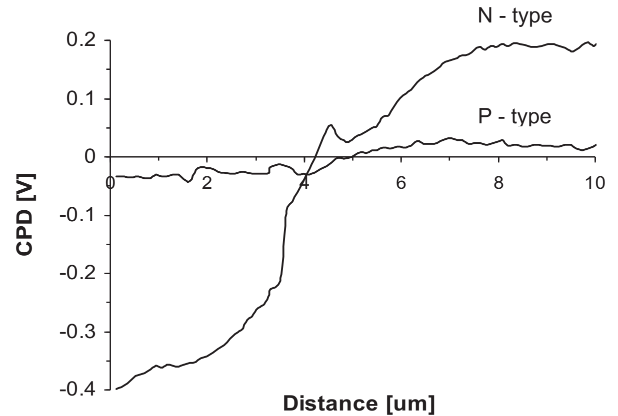

Fig. 6. The surface contact potential difference (CPD) across aluminum-doped p-type and n-type silicon wafers. The latter yields a ~0.5 V potential barrier.

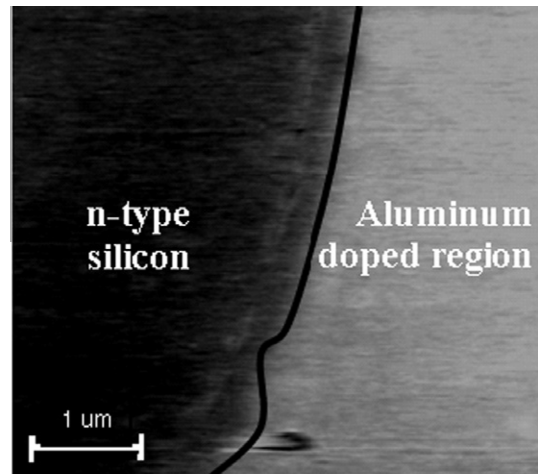

Fig. 7. The AFM surface potential image of the n-type silicon slice after point-contact microwave applicator treatment.

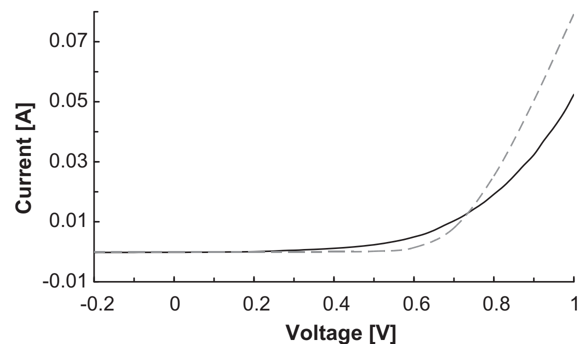

Fig. 8. The measured *I–V* characteristic of a silver-doped junction created by the point-contact microwave applicator (solid curve) in a comparison to an industrially manufactured *pn* junction (dashed curve).

ideal *pn*-junction. The potential difference was measured by AFM on the silver-doped silicon as well for three inserted RF power levels showing a linear dependence between the built-in voltage and the inserted RF power. The measured CPD's were 0.01, 0.17, and 0.30 V at 150-W, 250-W, and 350-W microwave power levels, respectively. The same measurements were conducted also prior to the microwave doping process in order to eliminate the possibility

that any potential difference had existed there before, and to verify that the original silicon surface structure was uncorrelated to the potential difference obtained by the doping process.

4. Analysis and discussion

The dopant atom concentration measured by SIMS can be approximated by

$$C_E = RSF_E \times \frac{I_E}{I_M} \quad (1)$$

where C_E is the dopant atom concentration per element, RSF_E is the dopant relative sensitivity factor for the relevant ion bombardment, e.g. cesium or oxygen as in our case, for each element (the RSF_E values for aluminum and silver is 1.4×10^{21} cm^{-3} and 7.2×10^{22} cm^{-3}, respectively [33]). I_E and I_M are the secondary ion intensities for the dopant and for the silicon matrix, respectively. The maximum atom concentrations were evaluated here as $\sim 5.5 \times 10^{19}$ cm^{-3} and 7.2×10^{22} cm^{-3} for aluminum and silver, respectively.

A one-dimensional (1D) approximation of the diffusion process can be obtained by the Fick Equation [1],

$$\frac{\partial C(x,t)}{\partial t} = D(T)\frac{\partial^2 C(x,t)}{\partial x^2} \quad (2)$$

where $C(x,t)$ is the impurity concentration, $D(T)$ is the diffusion coefficient, and x, t, and T are the position, time, and temperature, respectively. The solution of (2) is

$$C(x,\tau) = C_S \mathrm{Erfc}\left\{\frac{x}{2\sqrt{D(T)\tau}}\right\} \quad (3)$$

where C_s is the surface concentration, Erfc denotes the complementary error function, and τ is the total diffusion time assuming a constant temperature during the process. The result is depicted in Fig. 9 for the aluminum diffusion profiles with gross boundaries for temperatures of 1050 and 1100 °C resulting from Eq. (3) in a good agreement with the experimental result. Such agreement between this simplified model and the experimental results for aluminum doping was not achieved for silver doping in silicon.

The maximum achievable free-carrier concentrations are intrinsic properties of a given semiconductor [1,34]. In our case, the silicon matrix limits the formation of a highly doped p-type material. Though aluminum concentrations can reach the solubility limit in silicon [19], the resulting electrically-activated ion concentration for dopant atom densities above 10^{20} cm^{-3} is gradually saturated.

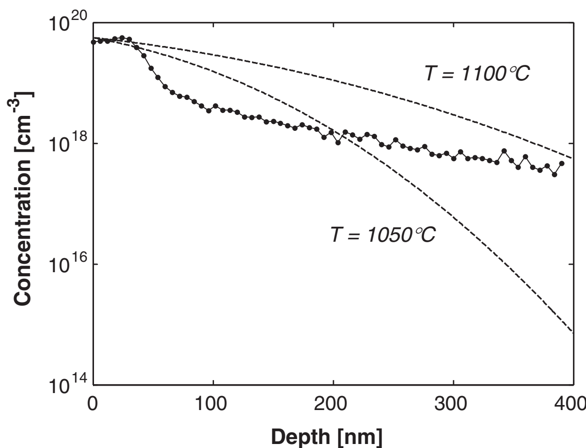

Fig. 9. The calibrated aluminum doping profile in silicon with the expected doping boundaries for temperatures of 1050 and 1100 °C obtained by the Erfc-function (3), in comparison with the experimental results.

The evaluation of relative atom densities in our doping experiment is achieved by SIMS measurements. Since the active ion concentrations for high levels of doping are not linearly dependent on the dopant atom densities, and the SIMS measurements account for total atom densities, an independent measurement (such as a Hall measurement) should be performed in order to evaluate the active ion densities [35].

The measurement of the junction built-in-voltage (Fig. 6) serves in this study as the independent method for estimating the electrically-activated ion concentrations. The maximal measured activated-ion concentration is deduced from this built-in potential by

$$N_A = \frac{n_i^2}{N_D}\exp\left(\frac{qV_{bi}}{KT}\right) \quad (4)$$

Where $n_i = 1.2 \times 10^{10}$ cm^{-3} is the intrinsic concentration at 300°K, $N_D \cong 8 \times 10^{14}$ cm^{-3} is the matrix donor concentration extracted from the surface resistivity ($R_s = 5\ \Omega$) [1], q is the electron charge, k is the Boltzmann coefficient, and $V_{bi} = 0.7$ V is the maximal *pn*-junction voltage, as measured by the AFM. As a result, the maximal activated atom concentration for both aluminum and silver doping is $N_A \sim 1 \times 10^{17}$ cm^{-3} for this barrier potential-difference.

Our experiments were performed in air atmosphere; therefore, three issues should be addressed concerning the results, namely (a) the influence of inherent oxygen impurities within the matrix over the concentrations evaluations, (b) the formation and influence of SiO_2 in the process over the doping process and profile, and (c) the validity of the Relative Sensitivity Factors (*RSF)* constants in the presence of SiO_2.

In a silicon matrix grown via the Czochralski method, in which the silicon is grown in a quartz crucible, some oxygen from the quartz diffuses into the silicon. These oxygen impurities form defects which give rise to donors in silicon. In the literature, these impurities, known as *thermal donors*, are actually double donor defects, having two donor electrons which can deactivate acceptor dopants. The concentration of these oxygen-derived donors is about 10^{18} cm^{-3} and they might cause a reduction in p-type doping efficiency at low doping levels [35]. In our experiment, the oxygen atom densities by SIMS measurement are above 10^{19} cm^{-3}. Therefore, the presence of inherent oxygen impurities in the silicon matrix itself (10^{18} cm^{-3}) is negligible for our preliminary estimations.

The formation of SiO_2 presented in Fig. 3a and b results from the doping process itself in air atmosphere. Due to the presence of SiO_2, the *RSF* values for the dopants might vary, hence presenting atom densities lower than really exist. Novak and Wilson [36] estimate the expected change in *RSF* values for Oxygen bombardment (as in our case) for Si and SiO_2 matrices, and present an extrapolated graph correlating the *RSF* for these two matrices with the ionization potential of the sputtered impurity. It is evident that the closer the ionization potential of the dopant is to that of Si ($\sim$8.16 eV), the expected change in *RSF* for the two matrices decreases. According to the extrapolation of [33], the estimated *RSF* for O^+ beam and SiO_2 matrix are 1×10^{22} cm^{-3} and 5×10^{22} cm^{-3} for aluminum and silver, respectively (with 5.99 and 7.58 eV ionization potentials, respectively). This indicates that for the dopants used, the presence of SiO_2 in the process of doping might present atom concentrations lower than the actual ones by a factor of $\sim$7 for aluminum and $\sim$1.5 for silver.

A better estimate for the change in measured concentrations in the presence of SiO_2 while using an Si matrix was derived by Schueler et al. [37]. In their experiments, ion implantation was performed in a silicon matrix through a layer of SiO_2. The surface concentrations of the implanted atoms were estimated after the removal of the SiO_2 layer using standard *RSF* values (as well as TOF-SIMS). The conclusion extracted from [37] is that *RSF* values

Table 1
A comparison of the microwave point-contact doping to other methods.

Property	Method			
	Microwave point-contact doping (MPCD)	Ion implantation and RTP [42–44]	Pulsed plasma doping [45,46]	Laser doping [47,48]
Thermal processing	Intrinsic to the doping process	A necessary step after implantation	A necessary step after implantation	Intrinsic to the doping process
Thermal processing realization	The MPCD applicator	Additional RTA apparatus	Additional RTA apparatus	The laser
Attained temperatures	~1000–1200 °C (locally)	~900–1100 °C	~900–1100 °C	~1420 °C (locally)
Dopants' penetration depth	0.01–0.3 μm	0.01–1 μm	0.01–0.1 μm	0.005–0.1 μm
Penetration depth controls	Microwave power, exposure time	Ion accelerating voltage, beam current	Bias pulse duty-cycle ratio	Pulse repetition, energy density, wavelength
Lateral profile controls	Doping tip diameter, exposure time	Ion beam profile	Gas flow rate, discharge voltage, time	Laser energy density, process time
Dopant's concentration controls	Microwave power, exposure time	Dopant dose, energy	Process time, pulse repetition, discharge power	Pulse repetition, wavelength, precursor gas chemisorbed
Complexity	Relatively simple	Complicated, sophisticated	Intermediate	Intermediate
Cost	Relatively low	High	Medium	Medium–High
Safety hazards	Microwave leak (unlikely)	High voltage, toxic gases	High voltage	Vapors

can be used for SiO_2 contaminated surfaces, and a mean standard-deviation of up to 20% in the measured concentrations can be expected. It is noted also that oxidation may impede doping processes [38–40].

5. Conclusions

Our experiments demonstrate the principle feasibility of the microwave point-contact concept for local doping and oxidation in silicon. The results show that using the modified microwave-drill device, both silver and aluminum can diffuse relatively fast up to depths of 0.3-μm, which are rather large depths in terms of the typical depth of shallow junctions in silicon submicron transistors. The diffusion time of one minute under a local microwave radiation is comparable to that of the other methods discussed below. Since accepted models of diffusion only partly corroborate these results, experiments should be performed, especially with silver doping, as well as with other dopants, also in vacuum conditions or nitrogen flow, in order to separate the doping and oxidation effects.

The rapid thermal diffusion processes of aluminum and silver in silicon achieved by the microwave point-contact applicator (Figs. 3–5) occur basically in non-equilibrium condition. Therefore, a simplified steady-state 1D model yields only rough estimates, as in Fig. 9 for the aluminum doping. Further experiments shall be followed by more comprehensive numerical analyses (e.g. [41]) to give a better theoretical insight of the experimental results.

Future experiments shall address also the issue of miniaturization; possibly by using an AFM as a platform for the point-contact microwave applicator. In this scheme, an AFM tip made of the doping material will radiate the near-field focused microwaves in order to obtain narrower junctions (in analogy to [23]). The local doping concept presented here can be incorporated with other capabilities of modified microwave drills (e.g. local heating, bonding [25], cutting, grooving, etc.). These could be applicable for small-scale (single chip) manufacturing [16], for MEMS fabrication, and for solid-state structuring processes [24].

A comparison of the proposed microwave-point-contact doping (MPCD) concept to the existing doping methods is shown in Table 1 for ion implantation [42–44], plasma doping [45,46], and laser doping [47,48]. It is evident now that using the MPCD setup it is possible to obtain junctions (with controllable profiles) comparable to that of mature methods. However, unlike ion implantation and plasma doping, the MPCD does not require additional tools to carry out the essential thermal processes for dopants activation and annealing. The thermal process proposed here is an intrinsic enabler of the junction creation. The MPCD setup is considerably simpler and cheaper with regard to sophisticated ion implanters and plasma doping equipment. Moreover, there is no need for hazardous high-voltages. Unlike existing RTP methods, the MPCD enables heating silicon locally as the laser based doping method. The MPCD junctions are accomplished with lower temperatures relative to the laser doping, which requires more complicated and expensive setups. It should be noted though that the MPCD at this premature stage of development has inferior lateral junction resolution with regard to ion implantation. Hence, the MPCD can be considered for applications which are less sensitive to spatial resolution of the formatted junctions yet requiring low-cost small-scale capabilities.

Acknowledgements

We thank Mr. I. Torchinsky for the AFM measurements, and Professors N. Croitoru, E. Glickman, E. Grunbaum, S. Krilov, A. Ruzin, and D.J. Chadi for helpful discussions. This research was supported by The Israel Science Foundation (Grant No. 1270/04). The authors request to dedicate this work to the memory of the late Dr. Vladimir Dikhtyar, who contributed significantly to this study and to other scientific and technological developments as well.

References

[1] S.M. Sze, Physics of Semiconductor Devices, Wiley, New York, 1981.
[2] International Technology Road Map for Semiconductors (ITRS), 2009 Edition, http://www.itrs.net.
[3] J.P. Castillo, A.T. Jacome, O. Malik, N.T. Lopez, Very shallow boron junctions in Si by implantation and SOD diffusion obtained by RTP, Microelectronics Journal 39 (2008) 678–681.
[4] J. Foggiato, W.S. Yoo, Implementation of flash technology for ultra shallow junction formation: challenges in process integration, Journal of Vacuum Science and Technology B 24 (2006) 515–520.
[5] P.K. Chu, Semiconductor applications of plasma immersion ion implantation, Plasma Physics and Controlled Fusion 45 (2003) 555–570.
[6] J.C.N. Reis, A.F. Beloto, M. Ueda, Annealing effects in samples of silicon implanted with helium by plasma immersion ion implantation, Nuclear Instruments and Methods in Physics Research Section B 240 (2005) 219–223.
[7] C.G. Jin, Y. Sasaki, K. Okashita, H. Tamura, H. Ito, B. Mizuno, K. Tsutsui, S. Ohmi, H. Iwai, Ultra shallow p^+/n junction formation by plasma doping (PD) and long pulse all solid-state laser annealing (ASLA) with selective absorption modulation, Nuclear Instruments and Methods in Physics Research Section B 237 (2005) 58–61.
[8] S.D. Kim, C.M. Park, J.C.S. Woo, Formation and control of box-shaped ultra-shallow junction using laser annealing and pre-amorphization implantation, Solid-State Electronics 49 (2004) 131–135.

[9] E. Takii, T. Eto, K. Kurobe, K. Shibahara, Ultra-shallow junction formation by green-laser annealing with light absorber Japanese, Japanese Journal of Applied Physics Part 2 (Letters) (44) (2005) 756–759.
[10] A. Florakis, A. Papadimitriou, N. Chatzipanagiotis, D. Tsoukalas, N. Misra, C. Grigoropoulos, Formation of silicon ultra shallow junction by nonmelt excimer laser treatment Proc. 39th European Solid-State Device Research Conf. (2009) 284–287.
[11] F. Sarubbi, T.L.M. Scholtes, L.K. Nanver, Chemical vapor deposition of boron layers on silicon for controlled nanometer-deep $p^{+}n$ junction formation, Journal of Electronic Materials 39 (2) (2010) 162–173.
[12] C.J. Bonifas, K. Thompson, J.H. Booske, R.F. Cooper, An examination of athermal photonic effects on boron diffusion and activation during microwave rapid thermal processing, Journal of Microwave Power and Electromagnetic Energy 42 (2008) 23–34.
[13] H. Noh, K. Moon, A. Cannon, J. Hesketh, C.P. Wong, Wafer bonding using microwave heating of parylene intermediate layers, Journal of Micromechanics and Microengineering 14 (2004) 625–631.
[14] N. Budraa, B. Ng, D. Wang, S. Ahsan, Y. Zhang, J. Mai, Microwave techniques for high-density electronics interconnect bonding and hybridization, IEEE Transactions on Nuclear Science 51 (2004) 3038–3042.
[15] R.B. James, P.R. Bolton, R.A. Alvarez, W.H. Christie, R.E. Valiga, Melting of silicon surfaces by high-power pulsed microwave radiation, Journal of Applied Physics 64 (1988) 3243–3253.
[16] R. Singh, R. Thakur, Chip making's singular future, IEEE Spectrum (2005) 36–41.
[17] H.F. Wolf, Silicon Semiconductor Data, Pergamon Press, 1969. pp. 136–140.
[18] R.B. Fair, Concentration profiles of diffused dopants in silicon, in: F.Y. Wang (Ed.), Impurity Doping, North Holland, 1981, pp. 387-389.
[19] D. Nagel, C. Frohne, R. Sitting, Applied Physic A (60) (1995) 61–65.
[20] D. Nagel, U. Kuhlmann, R. Sitting, Pn junction in silicon with blocking capabilities beyond 2.5 kV produced by rapid thermal processing, Solid-State Electronics 39 (1996) 965–970.
[21] H.H. Weitering, J.P. Sullivan, R.J. Carolissen, R. Pérez-Sandoz, W.R. Graham, R.T. Tung, Inhomogeneous Schottky barriers at Ag/Si(1 1 1) and Ag/Si(1 0 0) interfaces, Journal of Applied Physics 79 (1996) 7820–7829.
[22] N.J. Speer, S.J. Tang, T. Miller, T.C. Chiang, Coherent electronic fringe structure in incommensurate silver-silicon quantum wells, Science (314) (2006) 804–806.
[23] F.J. Rueß, K.E.J. Goh, M.J. Butcher, T.C.G. Reusch, L. Oberbeck, B. Weber, A.R. Hamilton, M.Y. Simmons, Narrow, highly P-doped, planar wires in silicon created by scanning probe microscopy, Nanotechnology (18) (2007) 1–5.
[24] P. Wilson, T.C.G. Reusch, S. Giordano, F.J. Rueß, A.R. Hamilton, M.Y. Simmons, Electrical characterization of ordered Si:P dopant arrays, IEEE Transactions on Nanotechnology 6 (2007) 213–217.
[25] E. Jerby, V. Dikhtyar, O. Aktushev, U. Grosglick, The microwave drill, Science 298 (2002) 587–589.
[26] E. Jerby, O. Aktushev, V. Dikhtyar, Theoretical analysis of the microwave-drill near-field localized heating effect, Journal of Applied Physics (97) (2005) 034909.
[27] P. Livshits, V. Dikhtyar, and E. Jerby, Localized heating, melting, and drilling of silicon, 4th World Congress on Microwave and RF Heating Applications, AIChE Annual Meeting, Austin, Texas, November 4–7, 2004.
[28] E. Jerby, P. Livshits, A. Shahadi, V. Dikhtyar, A. Inberg, A point-contact microwave applicator for local doping in silicon, Proceedings of Global Congress Microwave Energy Applications, pp. 481–84, August 4–8, 2008, Otsu, Japan.
[29] R. Herskowits, P. Livshits, S. Stepanov, O. Aktushev, S. Ruschin, E. Jerby, Silicon heating by a microwave-drill apparatus with optical interferometric thermometry, Semiconductor Science and Technology 22 (2007) 863–869.
[30] G.H. Buh, H.J. Chung, J.H. Yi, I.T. Yoon, Y. Kuk, Electrical characterization of an operating Si pn-junction diode with scanning capacitance microscopy and Kelvin probe force microscopy, Journal of Applied Physics 90 (2001) 443–448.
[31] A. Doukkali, S. Ledain, C. Guasch, J. Bonnet, Surface potential mapping of biased pn junction with kelvin probe force microscopy: application to cross-section devices, Applied Surface Science (235) (2004) 507–512.
[32] A. Kikukawa, S. Hosaka, R. Imura, Silicon pn junction imaging and characterizations using sensitivity enhanced Kelvin probe force microscopy, Applied Physics Letters 60 (1995) 3510–3512.
[33] R.G. Wilson, S.W. Novak, Systematics of secondary-ion-mass spectrometry relative sensitivity factors versus electron affinity and ionization potential for a variety of matrices determined from implanted standards of more than 70 elements, Journal of Applied Physics (69) (1991) 466–474.
[34] W. Walukiewicz, Defects and Self-Compensation in Semiconductors, Springer, Berlin, 2006 (Chapter 3) pp. 35–4.
[35] D.J. Chadi, Private communication, June 2007.
[36] S.W. Novac, R.G. Wilson, Systematics of positive secondary ion mass spectroscopy relative sensitivity factors for Si and SiO_2 measured using oxygen and argon ion bombardment, Journal of Applied Physics 69 (1991) 463–465.
[37] B.W. Schueler, C.N. Granger, L. McCaig, J.M. McKinley, J. Metz, I. Mowat, D.F. Reich, S. Smith, F.A. Stevie, M.H. Yang, Surface metal standards produced by ion implantation through a removable layer, Applied Surface Science (203-204) (2003) 847–850.
[38] B.I. Boltaks, H. Shih-Yin, Diffusion, solubility and the effect of silver impurities on electrical properties of silicon, Soviet Physics Solid State (2) (1961) 2383–2388.
[39] H. Bracht, Diffusion mechanisms and intrinsic point-defect properties in silicon, MRS Bulletin 25 (2000) 22–27;
. See alsoH. Bracht, Diffusion mediated by doping and radiation-induced point defects, Physica B 376–377 (2006) 11–18.
[40] J.C.C. Tsai, Diffusion, in: VLSI Technology, S.M. Sze (Ed.), McGraw-Hill, New York, 1983, pp. 169–218..
[41] S.A. Freeman, J.H. Booske, R.F. Cooper, Modeling and numerical simulation of microwave-induced ionic transport, Journal of Applied Physics 83 (1998) 5761–5772.
[42 E. Chason, S.T. Picraux, J.M. Poate, J.O. Borland, M.I. Current, T. Rubia, D.J. Eaglesham, O.W. Holland, M.E. Law, C.W. Magee, J.W. Mayer, J. Melngailis, A.F. Tasch, Ion beams in silicon processing and characterization, Journal of Applied Physics 81 (1997) 6513–6561.
[43] M.I. Current, Ion implantation for silicon device manufacturing: A vacuum perspective, Journal of Vacuum Science and Technology A Vacuum Surfaces and Films (14) (1996) 1115–1123.
[44] E. Rimini, Ion Implantation: Basics to Device Fabrication, Kluwer Academic Publishers, Boston, 1995.
[45] S.B. Felch, Z. Fang, B.W. Koo, R.B. Liebert, S.R. Walther, D. Hacker, Plasma doping for the fabrication of ultra-shallow junctions, Surface and Coatings Technology (156) (2002) 229–236.
[46] F. Lallementa, A. Grouilleta, M. Juhela, J.P. Reynarda, D. Lenoblea, Z. Fangb, S. Waltherb, Y. Raultb, L. Godetb, J. Scheuerb, Fabrication of N^{+}/P ultra-shallow junctions by plasma doping for 65 nm CMOS technology, Surface and Coatings Technology (186) (2004) 17–20.
[47] T. Sarnet, G. Kerrien, N. Yaakoubi, A. Bosseboeuf, E. Dufour-Gergam, D. Dé barre, J. Boulmer, K. Kakushima, C. Laviron, M. Hernandez, J. Venturini, T. Bourouina, Laser doping for microelectronics and microtechnology, Applied Surface Science (247) (2005) 537–544.
[48] G. Kerrien, T. Sarnet, D. Débarre, J. Boulmer, M. Hernandez, C. Laviron, M.N. Semeria, Gas immersion laser doping (GILD) for ultra-shallow junction formation, Thin Solid Films 454 (2004) 106–109.